Journal of The Electrochemical Society, **158** (11) E107-E110 (2011)
0013-4651/2011/158(11)/E107/4/$28.00 © The Electrochemical Society

Electrochemical Deposition Mechanism for ZnO Nanorods: Diffusion Coefficient and Growth Models

M. D. Reyes Tolosa,*,z J. Orozco-Messana, A. N. C. Lima, R. Camaratta, M. Pascual, and M. A. Hernandez-Fenollosa

Polytecnhnic University of Valencia, Instituto de Tecnología de Materiales, Camino de Vera s/n, Valencia 46022, Spain

Fabrication of nanostructured ZnO thin films is a critical process for many applications based on semiconductor devices. So on understanding of the electrochemical deposition mechanism is also fundamental for knowing the optimal conditions on growth of ZnO nanorods by electrodeposition.

In this paper the electrochemical mechanism for ZnO nanorods formation is studied. Results are based on the evolution of the diffusion coefficient using the Cotrell equation, and different growth models proposed by Scharifcker and Hills for nucleation and growth.

Manuscript submitted May 26, 2011; revised manuscript received July 26, 2011. Published October 5, 2011.

A broad range of high-technology applications, ranging from surface acoustic wave filters, photonic crystals, light emitting diodes, photodetectors, photodiodes, optical modulator waveguides, varistors, and gas sensor to solar cells, are based on ZnO nanostructures, due to its wide bandgap, excellent chemical and thermal stability, and its specific electrical and optoelectronic property of being a II-VI semiconductor with a large exciton binding energy.[1]

ZnO thin films have been prepared by a wide variety of techniques such as pulsed laser deposition,[2] sputtering,[3] and electrodeposition.[4] In particular, the electrodeposition technique has advantages over other processes due to its simplicity, low equipment cost and the possibility of obtaining large area thin films.[5] Also electrodeposition is an efficient and reliable technique for preparing ZnO nanocrystallites, nanowires and nanofibers.

There have been many reports on the electrodeposition of ZnO using aqueous[6–8] and non aqueous routes.[9] Most of the reported work on electrodeposition was done using solutions based on $ZnCl_2$ and $Zn(NO)_3$, in aqueous solution. Though the temperature required for the synthesis is important, the same as ion concentration, the morphology of the ZnO grown depends really on nucleation leading from unoriented polycrystalline films,[10,11] to nanorods[6] and sheets.[9] A key issue is the relation of electrochemical variables on nucleation for controlling the morphology of these films.[12]

The aim of this study is to determine the electrochemical growth mechanism for ZnO nanorods in a $ZnCl_2$ $5 \cdot 10^{-3}$M, KCl 0.1M solution, at different temperatures. As shown by Pauporté and Lincot[12] the electrochemical reactions that compete in the nucleation stage are:

$$Zn^{+2} + 0,5\,O_2 \rightarrow 2e^- + ZnO \qquad [1]$$

$$ZN^{+2} + H_2O + 0,5\,O_2 \rightarrow 2e^- Zn(OH)_2 \qquad [2]$$

This paper analyzes the kinetic control for both reactions at different temperatures and proposes a nucleation model mechanism for ZnO nanostructures. Through the presented models a better control of electrodeposited ZnO morphology can be attained.

Experimental

Samples were prepared from ITO sputtered glass (resistivity at room temperature 10 (Ω/cm^2). The substrates were cleaned using ultrasonic agitation in a mixture of distilled water with liquid neutral soap during 10 minutes, rinsing in distilled water for 10 minutes, and finally immersion in isopropanol for 10 minutes prior to drying in nitrogen current.

For the experiment a solution containing the following electrolytes was used: 0,1 M KCl Rectapur purity > 99%), ZnCl2 $5 \cdot 10^{-3}$ M (Panreac purity > 98%), and continuous oxygenation by a bubbling flow of 0,1 l/min of commercially pure oxygen. The electrochemical experiments were performed potentiostatically in a 3 electrode electrochemical cell with the substrate as cathode, a Pt sheet as counter electrode and a Ag/AgCl electrode (SE) as the reference electrode (VSE = 0,2 (13)). The potentiostat used was an Autolab PGSTAT302N with an ADC10M card for ultra fast measurement acquisition (1 sample every 10 ns).

All the experiments were made for 30, 40, 50, 60, 70 and 80 Celsius degrees.

Results

Cyclic Voltammetry.— As a starting point, the cyclic voltammetry curve has been analyzed in order to identify the potential for the different reactions between the working electrode (ITO sputtered glass) and the solution.

Cyclic voltammetry curves were obtained for each working temperature with a sweep rate of 0.1Volts per second. For each curve the two reactions according to 12 appear and are identified. Figure 1 shows cyclic voltammetry curves for the oxidation region at different working temperatures.

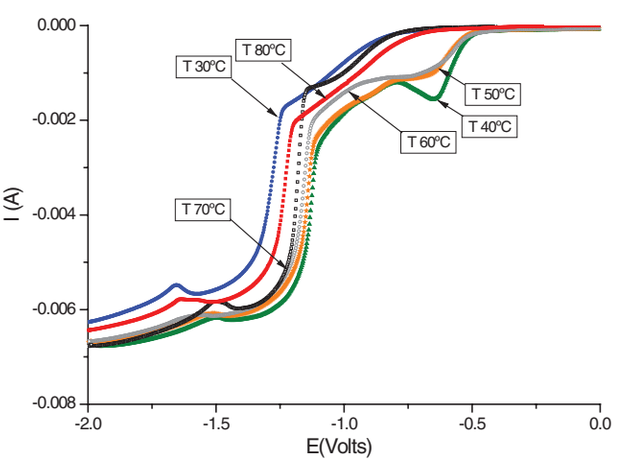

Figure 1. Oxidation region of cyclic voltammetry curves of $ZnCl_2$ $5 \cdot 10^{-3}$ M and KCl 0.1M solution for each working temperatures. Scan rate 0.1Volts/s.

* Electrochemical Society Student Member.
z E-mail: mareto@upvnet.upv.es

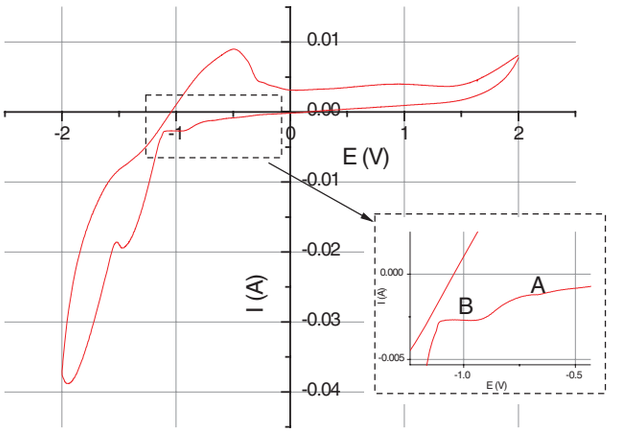

Figure 2. Cyclic Voltammetry curve of $ZnCl_2$ $5 \cdot 10^{-3}$M and KCl 0.1M solution, at 70°C. The Zinc hydroxides (A) and Zinc oxide (B) formation reactions are showed in detail.

Table I. Reaction potential for Zn(OH)n and ZnO formation.

T(°C)	E(Zn(OH)n) (V)	E(ZnO)(V)
30	− 0.8	− 1.2
40	− 0.55	− 1.2
50	− 0.55	− 1.1
60	− 0.8	− 1.1
70	− 0.7	− 1
80	− 0.8	− 1.05

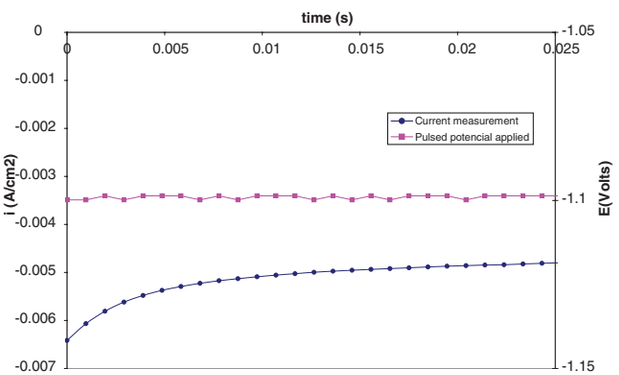

Figure 3. Current transient obtained for a voltage pulse, E(ZnO), applied at 50°C in a $ZnCl_2$ $5 \cdot 10^{-3}$M and KCl 0.1M solution.

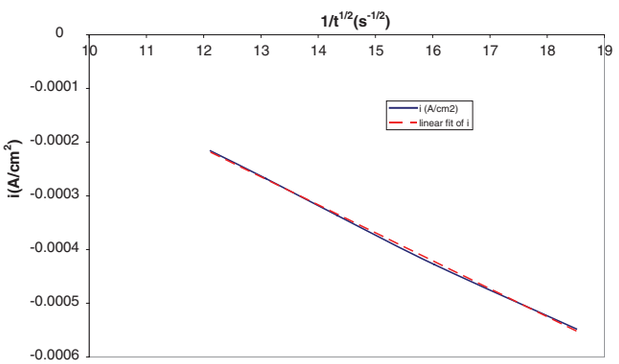

Figure 4. Cotrell plot used for determination of the diffusion coefficient of Zn^{+2} in the formation of $Zn(OH)_n$ at T = 30°C when a voltage pulse is applied.

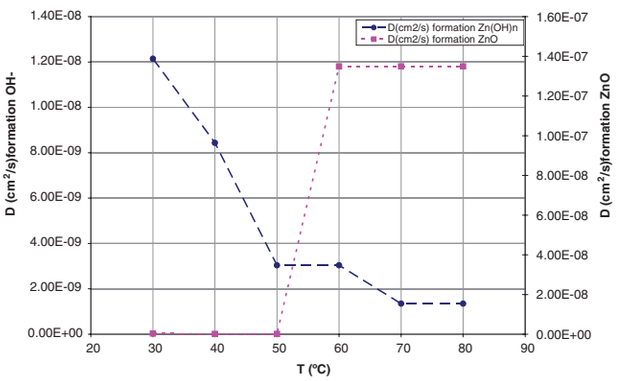

Figure 5. Diffusion coefficient obtained from Cotrell equation, for Zn^{+2} in both reactions 12, at different temperatures.

Reactions [1] and [2] are in competition within the electrochemical system. Initially, the formation of Zinc hydroxide takes place, followed at higher potentials by Zinc oxide formation, as shown on figure 2.

The Zinc hydroxide and ZnO formation potentials were registered for each working temperature, and are summarized in table I. Note, that all potentials are measured relative to the reference potential of Ag/AgCl electrode.

Electrochemical kinetics: Diffusion of electroactive species in solution.— When a constant reducing potential is applied to an electrode, the relationship between current density *i*, and time *t*, is known as the Cotrell equation.[14] For a reduction reaction and before the occurrence of the limiting current, it can be written:

$$i = \frac{n \cdot F \cdot D_0^{1/2} \cdot C_0^*}{\pi^{1/2} \cdot t^{1/2}} \qquad [3]$$

Where *i* is the cathodic current density, n represents the number of electrons exchanged, F is the Faraday constant, D_0 is the diffusion coefficient, and C_0^* is the concentration of the Zn^{+2} species to be reduced. By plotting $i = f(t^{-1/2})$, a linear graph is obtained until the growing diffusion layer has reached its maximum width.

The diffusion coefficient can then be determined by analysis of the potentiostatic current transient displayed in Figure 3.

At the beginning of the potentiostatic experiment, a non-Faradic current can be noticed due to the charging of the double layer. Therefore, the linear domain to be analyzed is after this non-Faradic interval.

The linear part of the experimental Cotrell plot can be seen on Figure 4, as well as the corresponding data fit.

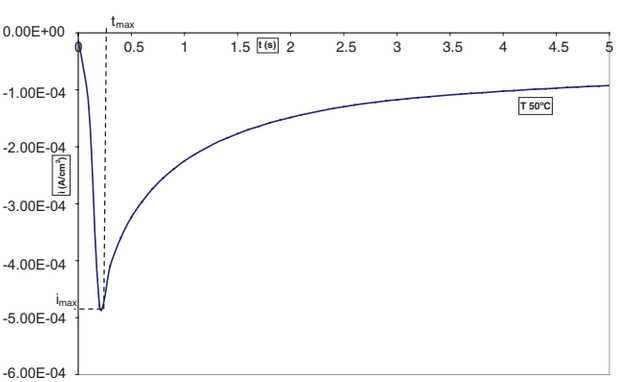

Figure 6. Current transient when a voltage pulse, E(Zn(OH)n), is applied to the ITO electrode at 50°C.

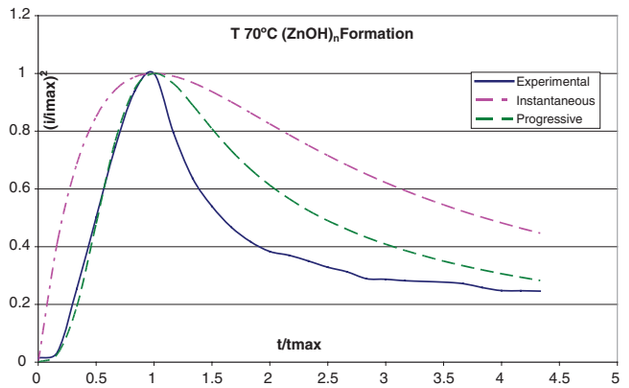

Figure 7. Theoretical models for $Zn(OH)_n$ nucleation compared to experimental data at 70°C.

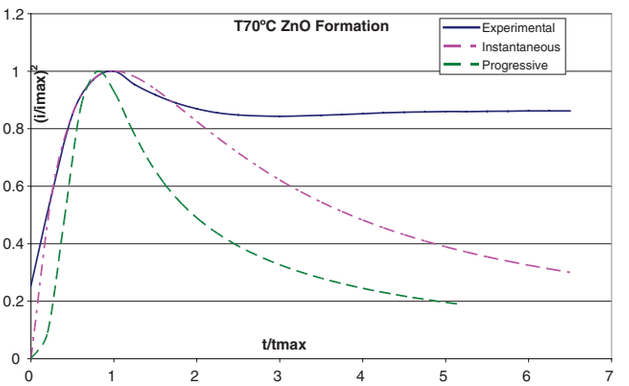

Figure 8. Theoretical models for ZnO nucleation compared to experimental data at 70°C.

This correlation was obtained for each working temperature, and each reaction (Zn(OH)n and ZnO formation), obtaining the diffusion coefficient for the Zn^{+2} ion, in each electrochemical reaction, see figure 5.

It is clearly seen on figure 5 that on the interval from 50 to 60 degrees Celsius there is an inversion on the reaction kinetics from hydroxide to ZnO formation. Experimentally, it has been established[12,13] that below 50°C there is no ZnO electrodeposition the reason is that the hydroxides consume all available Zn^{+2} ions before they evolve to ZnO.

Nucleation and Growth of ZnO.— The mechanism for the nucleation of Zinc oxide nanorods can be investigated using electrochemical methods. Scharifcker and Hills[15] developed in the 1980's theoretical models for nucleation, and formulated relations that can be used for establishing different nucleation and growth models. Their approach is based on the analysis of the current transient evolution when a constant potential is applied to the electrode. Such an experimental current transient is shown on figure 6.

The model by Scharifker and Hills is based on the assumption that the mass transport process for creating and growing nuclei is achieved by spherical, rather than by unidimensional (linear), diffusion. This case is commonly known as 3D nucleation with diffusion-controlled growth.

The cathodic current increases rapidly as the nuclei surface increases or new nuclei are formed. This is seen on Figure 6, for the current transient curve before reaching the instant t_{max}. This current increase can be also due to the nuclei edge effect responsible for the decreasing of the diffusion zone observed during the nucleation step. This typical behavior, which is observed in the case of microelectrodes, is consistent with the formation of nanowires behaving as microelectrodes. During this stage of growth, the nuclei develop diffusion zones around themselves. As the diffusion zones overlap, the diffusion regime will change from a spherical to a rather linear diffusion. This corresponds to the decrease in the cathodic current down to the limiting current that corresponds to linear diffusion.

Table II. Best fit nucleation models for ZnO electrodeposition.

T(°C)	Zn(OH)n	ZnO
30	Progressive	Instantaneous
40	Progressive	Instantaneous
50	Progressive	Instantaneous
60	Progressive	Instantaneous
70	Progressive	Instantaneous
80	Progressive	Instantaneous

This theory provides a diagnose relationship allowing a discrimination between nucleation modes. It is possible to plot experimental curves in a non-dimensional basis by representing $(i/i\max)^2$ vs. $(t/t\max)$ and comparing them with theoretical curves.[16] Note that $i\max$ and $t\max$ are the experimental values of the maximum current and the associated time of occurrence.

According to Scharifker and Hills, a perfect instantaneous nucleation process should follow the law:

$$\left(\frac{i}{i_{\max}}\right)^2 = \frac{1.9542}{t/t_{\max}}\left\{1-\exp\left(-1.2564\left(\frac{t}{t_{\max}}\right)\right)\right\}^2 \qquad [4]$$

And a progressive nucleation process is described by the relation:

$$\left(\frac{i}{i_{\max}}\right)^2 = \frac{1.2254}{t/t_{\max}}\left\{1-\exp\left(-2.3367\left(\frac{t}{t_{\max}}\right)^2\right)\right\}^2 \qquad [5]$$

According to this theory, for each working temperature a voltage pulse for each reaction, E(Zn(OH)n) and E(ZnO), was applied to the ITO electrode, and the corresponding transient current was analyzed, obtaining i_{max} and t_{max} for each experiment. Following the Scharifker and Hills theory, the non-dimensional experimental curves can be associated to a nucleation model. The comparison between the experimental and the theoretical curves are shown for 30°C in figure 7.

In table II the best fit model is identified for each electrochemical reaction at different temperatures.

As can be seen on the table the nucleation type for both reactions 1 and 2, is different for all temperatures within the interval studied. Within the interval reaction 1 has a Progressive nucleation type while reaction 2 is instantaneous.

Conclusions

The fact that $Zn(OH)_n$ are needed as precursors for ZnO (12) gives us the basics for controlling the morphology of electrodeposited ZnO nanostructures. When electrodeposition is performed below 50°C the small diffusion coefficient of the ZnO instantaneous nucleation is practically non existent because all available Zn^{+2} near the electrode surface is consumed for the progressive growth of the $Zn(OH)_n$ layer.

The nucleation, distribution and growth of the ZnO nanostructures is determined by the availability of Zn^{+2} ions (slower kinetics for the formation of the $Zn(OH)_n$ seeds) and the nucleation mechanism for ZnO.

From 60 to 70°C the seeds are created homogeneously due to the step on the diffusion coefficient for that reaction. If the current is maintained, a gradient for Zn^{+2} ions appears near the electrode surface and a bigger share of the ions are consumed by the instantaneous reaction (ZnO growth) rather than for the progressive reaction

($Zn(OH)_n$ growth) as can be observed from the bigger current density required for the instantaneous reactions (see Figure 7 and 8).

If the current is applied in fast pulses the gradient in Zn^{+2} concentration disappears and a more uniform distribution of nanostructures appears, thanks to a better seeding by $Zn(OH)_n$ and slower ZnO growth.

At higher temperatures the $Zn(OH)_n$ formation is so slow that the morphology is not perfectly homogeneous and provides thicker ZnO columns.

References

1. Lionel Vayssieres, *Adv. Materials* **15**, 464–466, (2003).
2. G. H. Lee, *Solid State Commun*. **128**, 351, (2003).
3. T. W. Kim, K. D. Kwack, H. K. Kim, Y. S. Yoon, J. H. Bahang, H. L. Park, *Solid State Commun*, **127**, 635 (2003).
4. Daniel Lincot, *Thin Solid Films*, **487**, 40–48 (2005).
5. Lisha Zhang, Zhiganag Chen, Yiwen Tang, Zhijie Jia, *Thin Solid Films*, **492**, 24–29, (2005).
6. J. Cembrero, A. Elmanouni, B. Hartiti, M. Mollar, B. Mari, *Thin Solid Films*, **198**, 451–452 (2004).
7. L. Zhang, C. Zhigang, Y. Tang, Z. Jia, *Thin Solid Films*, **492**, 24, (2005).
8. Y. L. Liu, Y. C. Liu, Y. X. Liu, D. Z. Shen, Y. M. Lu, J. Y. Zhang, X. W. Fan, *Physica B*, **322**, 31, (2002).
9. F. Wang, R. Liu, A. Pan, L. Cao, K. Cheng, B. Xue, G. Wang, Q. Meng, L. Jinghong, Q. Li, Y. Wang, T. Wang, B. Zou, *Mater. Lett*. **61**, 2000, (2007).
10. L. Zhang, C. Zhigang, Y. Tang, Z. Jia, *Thin Solid Films*, **492**, 24, (2005).
11. Y. L. Liu, Y. C. Liu, Y. X. Liu, D. Z. Shen, Y. M. Lu, J. Y. Zhang, X. W. Fan, *Physica B*, **322**, 31, (2002).
12. T. Pauporte, D. Lincot, *Electrochimica Acta* **45**, 3345–3353(2000).
13. R. Könenkamp, R. C. Word, M. Godinez; *Nano Letters*, **5**, 2005 (2005).
14. Electrochemical methods, Fundamentals and applications. Allen J. Bard, Larry R. Faulkner, John Wiley & Sons, Inc, 2001.
15. B. Scharifker and G. Hills, *Electrochim. Acta*, **28**, 879, (1983).
16. Ilie Hanzu, Thierry Djenizian, Gregorio F. Ortiz, and Philippe Knauth, *J. Phys. Chem. C*, **113**, 20568–20575, (2009).